This article is a *Plant Cell* Advance Online Publication. The date of its first appearance online is the official date of publication. The article has been edited and the authors have corrected proofs, but minor changes could be made before the final version is published. Posting this version online reduces the time to publication by several weeks.

The *Arabidopsis* Intracellular Na^+/H^+ Antiporters NHX5 and NHX6 Are Endosome Associated and Necessary for Plant Growth and Development [W]

Elias Bassil,[a,1] Masa-aki Ohto,[a,1] Tomoya Esumi,[a] Hiromi Tajima,[a] Zhu Zhu,[a] Olivier Cagnac,[a] Mark Belmonte,[b] Zvi Peleg,[a] Toshio Yamaguchi,[a] and Eduardo Blumwald[a,2]

[a] Department of Plant Sciences, University of California, Davis, California 95616
[b] Department of Plant Biology, College of Biological Sciences, University of California, Davis, California 95616

Intracellular Na^+/H^+ antiporters (NHXs) play important roles in cellular pH and Na^+ and K^+ homeostasis in all eukaryotes. Based on sequence similarity, the six intracellular *Arabidopsis thaliana* members are divided into two groups. Unlike the vacuolar NHX1-4, NHX5 and NHX6 are believed to be endosomal; however, little data exist to support either their function or localization. Using reverse genetics, we show that whereas single knockouts *nhx5* or *nhx6* did not differ from the wild type, the double knockout *nhx5 nhx6* showed reduced growth, with smaller and fewer cells and increased sensitivity to salinity. Reduced growth of *nhx5 nhx6* was due to slowed cell expansion. Transcriptome analysis indicated that *nhx5*, *nhx6*, and the wild type had similar gene expression profiles, whereas transcripts related to vesicular trafficking and abiotic stress were enriched in *nhx5 nhx6*. We show that unlike other intracellular NHX proteins, NHX5 and NHX6 are associated with punctate, motile cytosolic vesicles, sensitive to Brefeldin A, that colocalize to known Golgi and *trans*-Golgi network markers. We provide data to show that vacuolar trafficking is affected in *nhx5 nhx6*. Possible involvements of NHX5 and NHX6 in maintaining organelle pH and ion homeostasis with implications in endosomal sorting and cellular stress responses are discussed.

INTRODUCTION

Na^+/H^+ antiporters (NHXs) play important roles in pH regulation, Na^+ and/or K^+ homeostasis, and the regulation of cell volume in cells of diverse organisms ranging from bacteria to humans. NHXs catalyze the electroneutral exchange of Na^+ or K^+ for H^+ using the electrochemical H^+ gradient to direct inward movement of Na^+ or K^+ in exchange for luminal H^+. NHXs are integral membrane proteins residing in the plasma membrane (Shi et al., 2000) and in endosomal compartments and vacuoles (Apse et al., 1999; Pardo et al., 2006; Apse and Blumwald, 2007; Hamaji et al., 2009). They belong to the monovalent cation/proton antiporter CPA1 family of transporters (Maser et al., 2001). With the exception of yeast, which contains a single NHX gene, all eukaryotes sequenced to date contain multiple isoforms of NHX-like proteins designated as Na^+/H^+ exchangers (NHEs) (Brett et al., 2005a). In mammalian systems, organelle-specific distribution of NHE isoforms are required for specialized subcellular functions (Orlowski and Grinstein, 2007).

In *Arabidopsis thaliana*, intracellular NHXs are encoded by a multigene family consisting of *NHX1* through *NHX6* and are classified into two subgroups (Pardo et al., 2006). Two additional members of the family, NHX7/SOS1 and NHX8, are plasma membrane bound and do not localize to endomembranes (Shi et al., 2002). Based on their amino acid similarity, NHX1 to 4 cluster into one group, while NHX5 and 6 cluster as a separate group (Yokoi et al., 2002; Aharon et al., 2003; Brett et al., 2005a; Pardo et al., 2006). NHXs play diverse roles in processes including pH homeostasis in flowers (Yamaguchi et al., 2001), cellular K^+ homeostasis (Leidi et al., 2010), cell expansion (Apse et al., 2003), vesicular trafficking and protein targeting (Bowers et al., 2000; Sottosanto et al., 2004; Brett et al., 2005b), as well as salt tolerance (Apse et al., 1999). Whereas NHX1 remains the most studied of the intracellular NHXs, the roles of NHX2 to 6 remain largely unknown.

NHX5 and NHX6 localization and function have been postulated on the basis of sequence similarity to NHEs (Brett et al., 2005a) and are thought to be functionally different from other intracellular NHXs. Phylogenetic analysis indicated that *NHX5* and *NHX6* belong to a clade of endosomal antiporters that include tomato (*Solanum lycopersicum*) Sl *NHX2*, yeast (*Saccharomyces cerevisiae*) Sc *NHX1*, and human (*Homo sapiens*) Hs *NHE6*, *7*, and *9* (Brett et al., 2005a; Pardo et al., 2006). The Sl NHX2 protein colocalized with prevacuolar compartment (PVC) and Golgi markers in both yeast and tomato (Venema et al., 2003), as well as to small vesicles expressed transiently in onion epidermal cells (Rodriguez-Rosales et al., 2008). Mammalian Hs NHE6, 7, and 9 are localized in early recycling endosomes, the *trans*-Golgi network (TGN), and late recycling endosomes, respectively (Numata and Orlowski, 2001; Nakamura et al., 2005;

[1] These authors contributed equally to this work.
[2] Address correspondence to eblumwald@ucdavis.edu.
The author responsible for distribution of materials integral to the findings presented in this article in accordance with the policy described in the Instructions for Authors (www.plantcell.org) is: Eduardo Blumwald (eblumwald@ucdavis.edu).
[W] Online version contains Web-only data.
www.plantcell.org/cgi/doi/10.1105/tpc.110.079426

Ohgaki et al., 2008), while in yeast, Sc Nhx1 localized to the PVC (Nass and Rao, 1998; Bowers et al., 2000; Ali et al., 2004; Brett et al., 2005b). Although these results would predict a subcellular localization of NHX5 and NHX6 in endosomes, TGN, and/or PVC in plants, direct evidence supporting their localization and function is lacking.

Here, we used a genetic approach to investigate NHX5 and NHX6 functions. We found evidence showing that NHX*5* and NHX6 are critical for cell expansion, proliferation, and response to salt. We also show that NHX5 and NHX6 are localized to motile endosomal compartments, likely to be the Golgi and TGN. Our data support the role of NHX5 and NHX6 in vesicular trafficking to the vacuole.

RESULTS

NHX5 and NHX6 Are Putative Endosomal Na^+ (K^+)/H^+ Antiporters Expressed throughout Plant Development

NHX5 is a protein of ~521 amino acids with a molecular mass of 57 kD, whereas NHX6 contains 535–amino acid residues with a molecular mass of 59 kD. Depending on the software used (TMHMM; http://www.cbs.dtu.dk/services/TMHMM/ or http://wolfpsort.org/), NHX5 is predicted to comprise between 9 and 10 putative transmembrane domains, whereas NHX6 is thought to have eight to nine transmembrane domains (see Supplemental Figure 1 online). A sequence comparison indicated that members of the group containing NHX1-4 are >51% similar among themselves, whereas NHX5 and NHX6 are >68% similar to each other but <30% similar to NHX1-4 (see Supplemental Figure 1 online).

The expression of *NHX5* and *NHX6* was examined in different organs and developmental stages. Both *NHX5* and *NHX6* were expressed in flowers, flower buds, stems, rosette leaves, and roots. The overall level of expression *NHX5* was slightly higher than that of *NHX6* except in siliques (see Supplemental Figure 2 online). The nearly ubiquitous expression of *NHX5* and *NHX6* could be confirmed in publicly available expression data (i.e., http://bbc.botany.utoronto.ca/efp/cgi-bin/efpWeb.cgi).

Generation of *nhx5 nhx6* Double Knockouts

To investigate the function of NHX*5* and NHX*6*, we generated knockout mutants using available T-DNA insertion lines. For each gene, two separate T-DNA lines were selected for single knockouts and designated as *nhx5-1*, *nhx5-2*, *nhx6-1*, and *nhx6-2* (see Methods). Single knockouts were genotyped and backcrossed two times before their subsequent use in crosses to generate the two independent double knockout lines *nhx5-1 nhx6-1* and *nhx5-2 nhx6-2* (see Supplemental Figure 3 online). Expression of *NHX5* and *NHX6* in all knockouts was confirmed with quantitative real-time PCR (qPCR; see Supplemental Figure 3 online). Furthermore, the expression of *NHX1*, *NHX2*, *NHX3*, and *NHX4*, as quantified by qPCR, did not change significantly in either single or double *nhx5 nhx6* knockouts (see transcriptional profiling section below).

The single knockouts *nhx5* and *nhx6* did not show any obvious growth phenotypes or developmental defects when grown in either soil (Figure 1) or plates (Figure 4; see Supplemental Figure 6 online). The double knockout *nhx5 nhx6*, however, displayed remarkable growth and developmental phenotypes (Figures 1A to 1D). Under either short (SDs) or long days (LDs), *nhx5 nhx6* was drastically smaller and displayed much slowed development compared with wild-type plants (Figures 1E and 1F). Growth differences became more pronounced over time such that at 35 d, the rosette diameter of *nhx5 nhx6* was 20% that of the wild type (Figure 1E). Compared with the wild type, double knockout plants bolted ~3.5 weeks later under LDs and did so at half the number of rosette leaves (Figure 1). In general, flowering time in *Arabidopsis* closely coincides with rosette leaf number. The *nhx5 nhx6* double mutant displayed a lack of correlation between flowering time and leaf number because it flowered temporally later but developmentally sooner, probably due to slowed cell proliferation. Also, root growth was similarly inhibited in *nhx5 nhx6* (see Supplemental Figure 4 online). All phenotypes discussed above were identical in both of the independently generated double knockouts lines investigated (i.e., *nhx5-1 nhx6-1* and *nhx5-2 nhx6-2*). Importantly, transformation of *nhx5 nhx6* with either C terminus–tagged *NHX5-YFP* (for yellow fluorescent protein) or *NHX6-GFP* (for green fluorescent protein) rescued the *nhx5 nhx6* phenotype because both *NHX5*-YFP *nhx5 nhx6* and *NHX6*-GFP *nhx5 nhx6* resembled the wild type/single knockouts (Figure 1G; see Supplemental Figure 5 online), thus indicating that C-terminal tagging of NHX5 or NHX6 did not affect protein function.

nhx5 nhx6 Displayed Decreased Leaf Cell Size and Cell Number but Unaltered Cell Identity

Given the slow growth and development of *nhx5 nhx6*, we sought to compare cellular organization and architecture in leaves. Cross sections through the midvein of *nhx5 nhx6* leaves revealed a profound reduction in cell size and number (Figure 2). Mesophyll cell size and cell number (Figures 2A to 2C) were reduced by almost 50% in the double knockout compared with the wild type. To determine if this effect was cell specific, we also quantified xylem cell size and number in the same cross sections and determined a similar trend (Figures 2D to 2F). The area of palisade mesophyll cells (calculated through a cross section) of leaf margins in *nhx5 nhx6* cells was 55% of that of wild-type palisade cells (Figures 2G to 2I). Similar to other cell types, the area of epidermal cells was also reduced. Quantitative estimates of cell area, calculated from images taken of epidermal peels, indicated that the average cell area of *nhx5 nhx6* was 26% of that of wild-type cells (Figures 2J to 2L). Secondary cell wall deposition as assayed by toluidine blue-O staining appeared considerably reduced in the double mutant (Figure 2E; blue color). Chloroplasts within mesophyll cells were stained with amido black 10B and appeared more concentrated in the double knockout (Figure 2H) probably because of the smaller cell size (Figure 2C), which correlated well with the dark green color seen in *nhx5 nhx6* leaves (Figure 1D). In *nhx5 nhx6* leaves, cells remained highly organized, suggesting that cell identity was not affected. These results indicate that NHX5 and NHX6 play

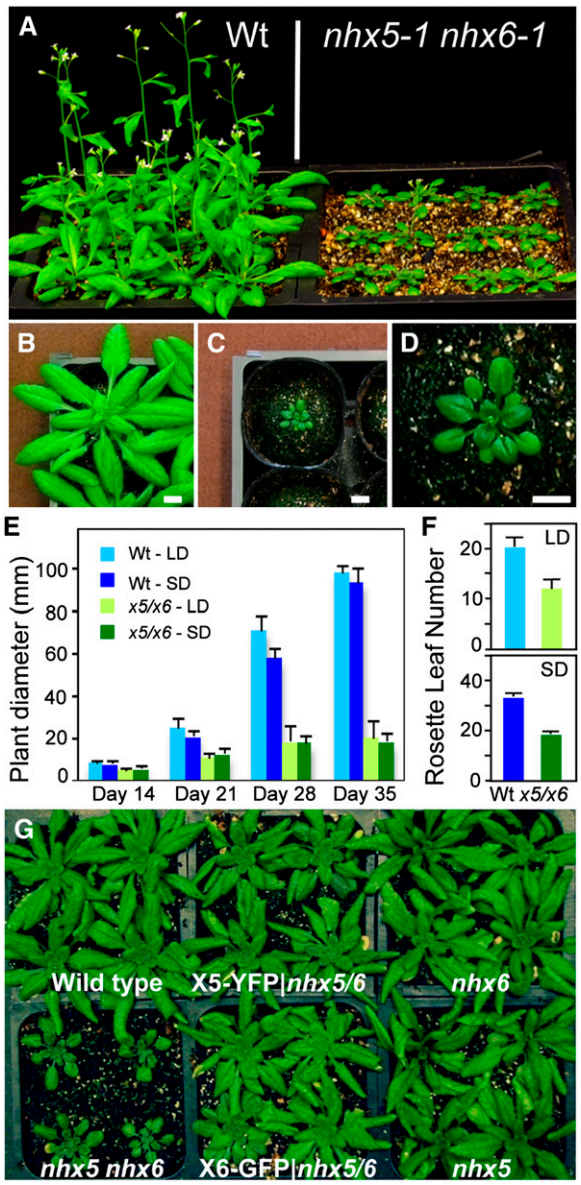

Figure 1. Growth and Development of *nhx5 nhx6* Double Mutants.

(A) Phenotype of *nhx5 nhx6* double mutants when grown on soil (14 d) under LDs (16 h light/8 h dark). Initially, plants were germinated on plates and grown for 14 d (12 h light/12 h dark) before transplanting to soil.
(B) to **(D)** Representative close-up images of individual wild-type **(B)** and *nhx5 nhx6* (**[C]** and **[D]**) plants taken at 35 d from planting and growth under LDs.
(E) Size of the wild type and *nhx5 nhx6* (average diameter of rosette) measured over 5 weeks of growth in LDs or SDs (8 h light/16 h dark).
(F) Visible number of rosette leaves of plants in **(E)** counted at 35 d after planting when plants are grown under either LDs (top panel) or SDs (bottom panel).
(G) Transformation of *nhx5 nhx6* (bottom left) with either NHX5-YFP (middle top panel) or NHX6-GFP (middle bottom panel) rescues the phenotype. The single knockouts *nhx5* and *nhx6* (right panels) and the wild type are included for comparison. Representative images of 5-week-old T2 transformants grown in soil are shown.
Bars = 1 cm in **(B)** to **(D)**. Error bars are SD; $n = 10$.

fundamental role(s) in cell proliferation and cell expansion that are not specific to cell differentiation.

Slower Tip Growth and Cytoplasmic Streaming in *nhx5 nhx6* Mutants

To obtain additional insight into the causes of the *nhx5 nhx6* phenotype, we made observations at the single-cell level. Elongating root hair cells are an excellent system to study dynamic processes because they grow rapidly and are highly dependent on profuse synthesis and trafficking of membrane and cell wall material. The growth of *Arabidopsis* on standing microscopic slides enabled the noninvasive live-cell imaging of individual cells (see Methods for more details). We measured root hair cell elongation by quantifying the rate of tip growth from time-lapse movies taken while the root hairs were under microscopy observation (see Supplemental Movie 1 online). For meaningful comparisons, only emerging root hair bulges from similar regions of the primary root elongation zone in actively growing seedlings were used. The average rate of tip growth (measured over 1 h) in *nhx5 nhx6* was considerably slower (0.23 ± 0.03 μm s^{-1}) than that of comparable wild-type root hairs (0.9 ± 0.14 μm s^{-1}) (Figure 3A). Similar to whole-plant growth, the cumulative length of root hair cells increased progressively over the observation period such that 60 min after emergence, wild-type root hair cells were 5 times longer than double knockout root hair cells (Figures 3B and 3C). Oscillations in the tip growth rates, due to the known pulse growth nature of hair cells (Hepler et al., 2001, also did not appear to be affected in *nhx5 nhx6* (Figure 3A). Time-lapse movies of extending hair cells, shown in Figure 3C, are included online (see Supplemental Movie 1 online).

Cytoplasmic streaming of actively growing wild-type root hair cells appears as a tip directed stream of cytoplasm intermixed with vacuolar strands. Both anterograde and retrograde cycling of vesicles to and from the tip are readily apparent. A comparison of such cytoplasmic streaming, however, indicated that in *nhx5 nhx6* root hairs, streaming appeared to be much slower and without its characteristic directionality toward the tip (i.e., lacking polarity) (see Supplemental Movie 2 online).

nhx5 nhx6 Is Salt Sensitive

Given the known role of NHX in salt responses (Apse et al., 1999), the sensitivity of *nhx5 nhx6* double mutants to salt stress was also investigated. When 2-week-old seedlings were transplanted from control media (1 mM NaCl) to 150 mM NaCl–supplemented plates and grown further for 2 weeks, growth differences between the double knockout and the wild type became evident (Figure 4). Before transplant, *nhx5 nhx6* had 70% of the fresh weight of wild-type plants, but after 2 weeks of growth on salt, fresh weight of *nhx5 nhx6* was only 43% of that of the wild type. The fresh weight of *nhx5 nhx6* at 150 mM NaCl was only 38% of that of plants grown on 1 mM NaCl, whereas in wild-type plants, fresh weight at 150 mM NaCl was 72% of that in 1 mM NaCl media. In contrast with *nhx5 nhx6*, the sensitivity to salt of the single knockouts *nhx5* and *nhx6* did not differ from the wild type (Figure 4). Interestingly other double knockouts combining *NHX5* and the vacuolar NHX members *NHX1* and *NHX3* (i.e., the double

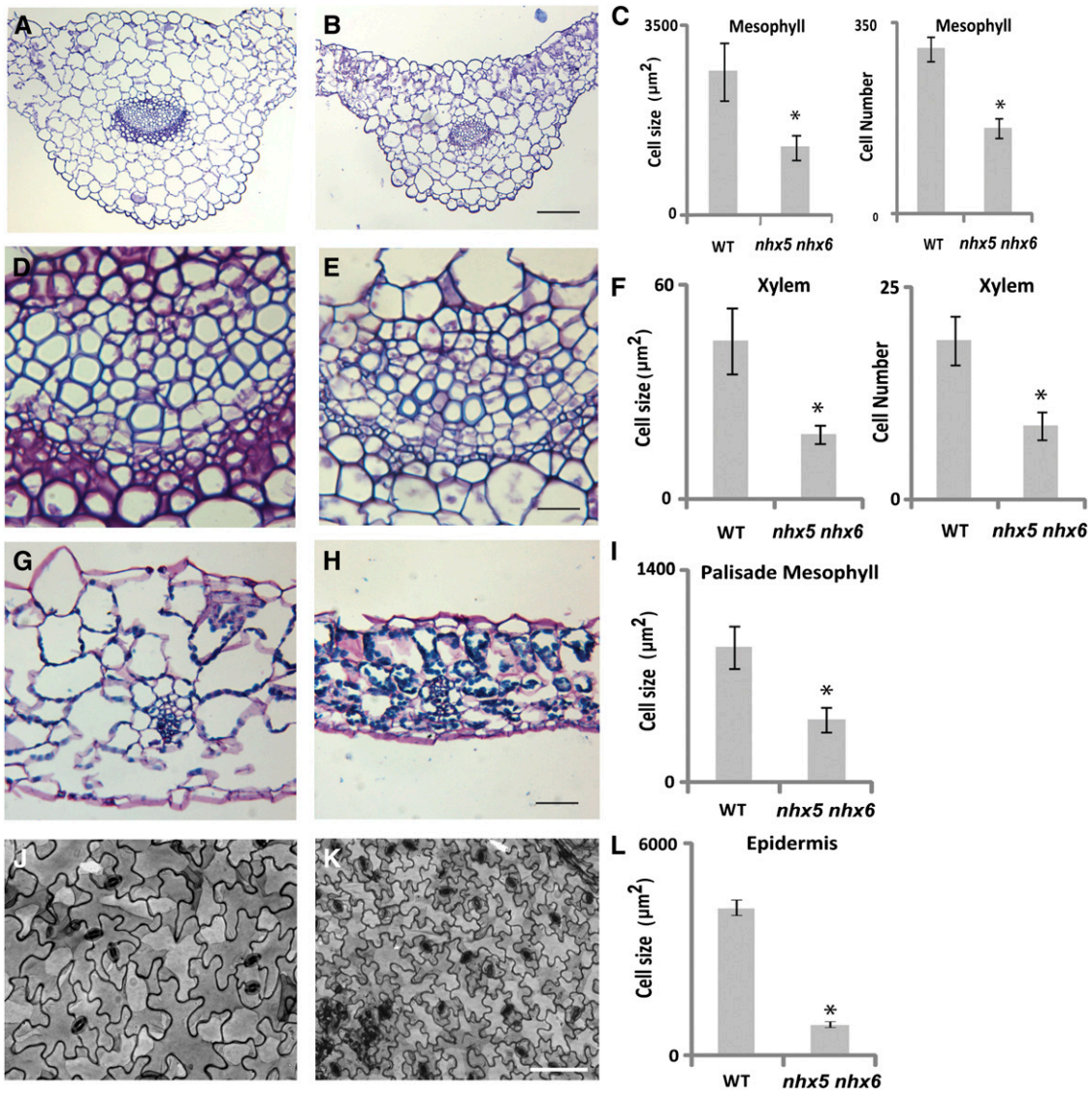

Figure 2. Anatomical Structure and Quantification of Cell Size and Cell Number in the Wild Type and the *nhx5 nhx6* Double Knockout.

(A) Median longitudinal section of a wild-type leaf.
(B) Median longitudinal section of an *nhx5 nhx6* leaf.
(C) Quantification of mesophyll cell size and number in the wild type and *nhx5 nhx6* determined from sections in **(A)** and **(B)**.
(D) High-magnification image of **(A)** shows secondary cell wall deposition (blue color) in vascular bundles as determined by toluidine blue-O staining.
(E) High-magnification section of **(B)** showing staining of vascular bundles in *nhx5 nhx6* (as described in **[D]**).
(F) Quantification of xylem diameter and vessel number in wild-type and *nhx5 nhx6* sections from **(D)** and **(E)**.
(G) Wild-type leaf cross section showing palisade mesophyll cells.
(H) *nhx5 nhx6* leaf cross section showing smaller palisade mesophyll cells.
(I) Quantification of palisade cell size in **(G)** and **(H)**.
(J) Epidermal peel of a wild-type leaf.
(K) Epidermal peel of an *nhx5 nhx6* leaf.
(L) Quantification of the area of epidermal cells in the wild type and *nhx5 nhx6* from peels in **(J)** and **(K)**.
(A), **(B)**, **(E)**, and **(F)** were stained with toluidine blue-O for secondary cell wall deposition and visualization of general histological organization of cells. Leaf margins were stained with periodic acid–Schiff for total carbohydrates and counterstained with amido black 10B for protein. At least 10 different leaf sections were used for the quantification of cell size and number. Bars = 80 μm in **(A)** and
(B), 10 μm in **(D)** and **(E)**, 30 μm in **(G)** and **(H)**, and 50 μm in **(J)** and **(K)**. Asterisks indicate significant difference ($P \leq 0.05$; *t* test). Error bars are SD; $n = 10$.

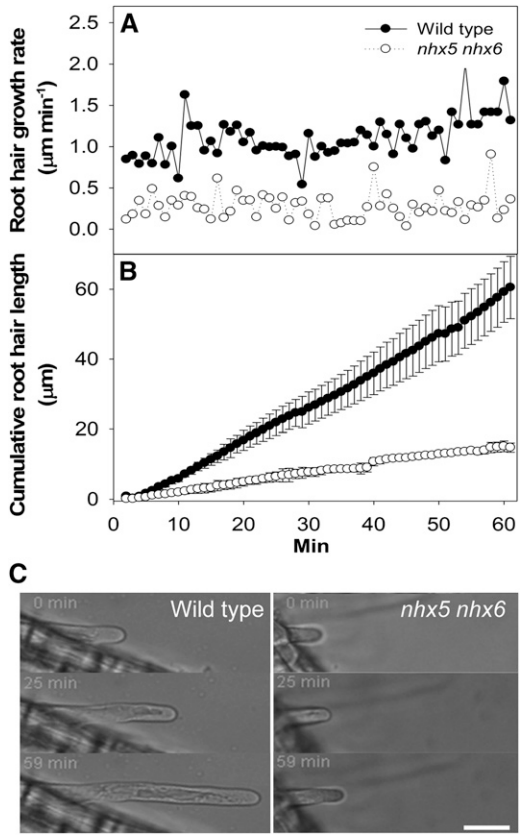

Figure 3. Rate of Tip Growth of Elongating Root Hair Cells in the Wild Type and the *nhx5 nhx6* Knockout.

(A) Root hair growth rate of representative hair cells from wild-type and *nhx5 nhx6* seedlings monitored over 1 h.

(B) Cumulative growth of root hairs from wild-type and *nhx5 nhx6* seedlings after 1 h of measurement.

(C) Images depicting the progression of wild-type and *nhx5 nhx6* root hair elongation at time 0, 25, and 59 min after measurement began.

Three-day-old seedlings, initially germinated on solidified media and then transferred to vertical slides (as described in Methods) were used for growth measurements. Seedlings were allowed to acclimate to new conditions for 12 h before selecting emerging root hair initials for growth measurements. Only seedlings showing vigorous root growth after acclimation were used, and the measurements were always performed at the same time of day. The wild type and *nhx5 nhx6* double knockouts were grown on the same slides. Elongation was estimated by tracking the extension of root hair tips in a sequence of acquired images using MetaMorph (Molecular Devices). Root hair lengths are the means (±SE of 10 root hairs) measured from 10 different seedlings. Corresponding time-lapse movies are included as Supplemental Movie 1 online.

knockouts *nhx1 nhx5* and *nhx3 nhx5*) also did not differ considerably from the wild type in their response to salt (see Supplemental Figure 6 online). At germination, *nhx5 nhx6* displayed even greater sensitivity to salt, evidenced by a nearly complete arrest of growth after cotyledon emergence, followed by slight, if any, seedling establishment when sown on 100 mM NaCl–supplemented plates (see Supplemental Figure 6 online).

Subcellular Localization of NHX5 and NHX6

To determine the subcellular localization of NHX5 and NHX6, we generated C-terminal translational fusions between cDNA sequences and YFP for NHX5 or GFP for NHX6, driven by the 35S promoter. All lines expressing NHX5-YFP and NHX6-GFP in the *nhx5 nhx6* background were indistinguishable from wild-type plants (Figure 1G), indicating that the fusion proteins were functional. We examined the fluorescence pattern in seedlings of at least six independently generated lines of NHX5-YFP and NHX6-GFP using confocal laser scanning microscopy. In all cell types examined, a punctate highly motile pattern, consistent with trafficking endosomal bodies, was found in both NHX5-YFP and NHX6-GFP (Figure 5; see Supplemental Figure 7 online). The reporter-associated signals for NHX5 and NHX6 were identical to each other in all independent lines examined. Particularly interesting were the prominent fluorescence patterns of trichomes, guard cells, and columella cells of the root tip and cells proximal to the quiescent center that were devoid of any detectable fluorescence (see Supplemental Figure 7 online). In elongating root hair cells, trafficking of NHX5 (and NHX6) positive bodies was especially rapid in both the anterograde and retrograde directions, as shown in Supplemental Movie 3 online. In all NHX5-YFP and NHX6-GFP lines examined, no signal associated with vacuoles was detected in any cell type observed. These data strongly support the notion that NHX5 and NHX6 reside in trafficking vesicles of the endomembrane system and not in vacuoles.

The lipophilic styryl dye FM4-64 is frequently used as a tracer for endocytotic trafficking and is a useful tool for endomembrane studies (Geldner et al., 2003; Samaj et al., 2005). Application of 4 μM FM4-64 to NHX5-YFP and NHX6-GFP resulted in a small fraction of NHX-positive bodies that colocalized with FM4-64–labeled endosomes when monitored after either 10 or 40 min (Figure 5B; see Supplemental Figure 8 online). Application of the fungal toxin Brefeldin A (BFA), a vesicle trafficking inhibitor (Nebenführ et al., 2002), caused the quick aggregation of NHX positive bodies into larger vesicular agglomerations, so-called BFA bodies, that were also costained with FM4-64 (Figures 5E to 5G). The response to BFA was identical in NHX5 and NHX6 reporter lines and was consistent with the notion that NHX5 and NHX6 may be localized to the Golgi, TGN, and/or other endosomal compartments.

To further asses NHX5 and NHX6 subcellular localization, crosses of NHX5-YFP and NHX6-GFP to other characterized reporters were performed. We selected VHA-a1, subunit a1 of the vacuolar H-ATPase (V-ATPase) (Dettmer et al., 2006), and SYP61, a syntaxin member of the SNARE family of proteins (Robert et al., 2008; Viotti et al., 2010), both TGN resident proteins, the syntaxin SYP32, a Golgi marker (Bassham et al., 2008; Geldner et al., 2009), as well as Sorting Nexin1 (SNX1), a marker of PVCs (Jaillais et al., 2008). Colocalization experiments of the resulting T1 double reporter seedlings, coexpressing combinations of NHX5 or NHX6 with the above-mentioned reporters, are shown in Figure 6. Quantification of the extent of colocalization was assessed as described in Methods using intensity correlation analysis (Li et al., 2004), which resulted in a quotient (ICQ) that was used to compare the relative colocalization between the different

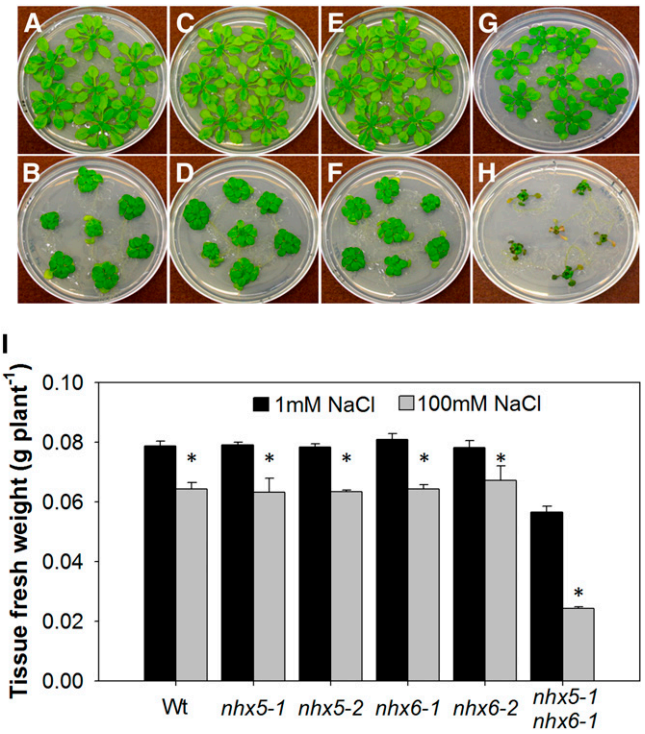

Figure 4. Response of Single and Double Knockouts of *nhx5* and *nhx6* to Salt.

Plants were sown on plates with 1 mM NaCl and grown for 14 d (12 h light/dark) and transplanted to new plates containing either 1 mM NaCl (**[A]**, **[C]**, **[E]**, and **[G]**) or 150 mM NaCl (**[B]**, **[D]**, **[F]**, and **[H]**) and grown for another 2 weeks.
(A) and **(B)** The wild type.
(C) and **(D)** The single knockout *nhx5-1*.
(E) and **(F)** The single knockout *nhx6-1*.
(G) and **(H)** The double knockout out *nhx5-1 nhx6-1*.
(I) Tissue fresh weight of single and double mutants of plants shown in **(A)** to **(H)**. Images of *nhx5-2* and *nhx6-2* are included in Supplemental Figure 4 online. Asterisks indicate significant difference between treatments for the indicated genotype ($P \leq 0.01$; *t* test). Values are the mean ± SD; $n = 12$.

double reporter lines. In root hair cells of NHX6-GFP VHA-a1-RFP, the fluorescence pattern of NHX6 and VHA-a1 overlapped significantly (ICQ = 0.397 ± 0.07), indicating high colocalization between the two proteins (Figures 6A to 6C). Addition of 25 μM BFA caused the aggregation of both NHX6-GFP and VHA-a1-RFP into characteristic BFA compartments containing both marker proteins (see Supplemental Figure 8F online). A similar high degree of colocalization was also observed between NHX5 and VHA-a1 (ICQ = 0.36 ± 0.09; Figures 6D to 6F). Colocalization between NHX6 and SYP32, the Golgi marker, was also substantial (ICQ = 0.411; Figures 6G to 6I), suggesting that NHX6 may also reside in the Golgi. The application of BFA to the NHX6 SYP32 double reporter indicated that NHX6 is more sensitive to BFA than SYP32 because we observed that NHX6 aggregated into BFA bodies sooner than did SYP32 and that NHX6 localized to the core of the bodies, whereas SYP32 decorated their periphery (see Supplemental Figure 8L online). In the double reporter NHX5-YFP SYP61-CFP, colocalization between NHX5 and SYP61 was significant (ICQ = 0.322 ± 0.08; Figures 6J to 6L); however, little colocalization between NHX6 and SNX1-positive bodies was seen in the double reporter NHX6-GFP SNX1-RFP (ICQ = 0.24 ± 0.06; Figures 6M to 6O), suggesting that NHX6 may not be significantly associated with the PVC. By transiently expressing NHX5-RFP in stably transformed NHX6-GFP plants, we found that NHX5 and NHX6 colocalized significantly (ICQ = 0.402 ± 0.09; Figures 6P to 6U).

The subcellular localization of NHX6 was confirmed using immunogold electron microscopy of thin sections of root tips probed with a GFP antibody. Gold particles associated with endomembranes near the TGN, as well as with vesicular bodies budding from the TGN, were clearly observed (Figures 6V and 6W). Cells of wild-type seedlings did not show labeling above background (Figure 6X). Taken together, these results suggested that NHX5 and NHX6 are associated with endosomal compartments of the Golgi and TGN but not with the PVC.

Trafficking to the Vacuole Is Affected in *nhx5 nhx6*

We used the endocytotic tracer FM4-64 to monitor further and compare endosomal trafficking between the wild type and *nhx5 nhx6*. In *Arabidopsis* root tip cells, FM4-64 initially labels the plasma membrane and becomes internalized into endosomal bodies that traffic throughout the endomembrane system before ending in the vacuole(s) (Samaj et al., 2005). Using actively growing (i.e., trafficking) roots, we monitored and compared the progression of endomembrane labeling in *nhx5 nhx6* root tip cells. To minimize any differences due to handling, wild-type and *nhx5 nhx6* seedlings were grown on the same slides and treated identically (described in Methods). Labeled endosomes became evident in both wild-type and *nhx5 nhx6* roots, ~15 min following FM4-64 application (arrows in Figures 7A and 7B). Under these conditions, labeling of vacuolar compartments in wild-type root tip cells occurred at ~70 to 80 min following FM4-64 application (arrowheads, Figure 7C), whereas in *nhx5 nhx6* root tip cells, labeling of vacuoles did not occur even after 95 min (Figure 7D). In fact, we consistently observed that in *nhx5 nhx6*, only minor labeling of vacuoles was evident, even after 180 min, with most FM4-64 label remaining predominantly as punctate endosomal bodies, similar to cells observed at 10 to 15 min after FM4-64 application (Figures 7A and 7B). The delay or lack of vacuolar staining in *nhx5 nhx6* suggested that the step from the TGN to a later endosomal compartment (PVC) or vacuole may be either inhibited or severely delayed. We also tested whether early endocytotic steps or recycling processes may be affected in *nhx5 nhx6* by pretreating roots with BFA before staining with FM4-64 and monitored for the progression of endomembrane labeling as above. In cells of BFA-treated root tips, large BFA bodies were visible within 15 min of FM4-64 labeling, in the wild type. In *nhx5 nhx6* roots, fewer, smaller BFA bodies formed and correlated to the fewer number of endosomal bodies observed in *nhx5 nhx6* (Figure 7B). BFA agglomerations also took considerably longer to form in *nhx5 nhx6* (30 min compared with 15 min in the wild type; Figures 7E and 7F). These data suggest that early endocytotic steps and processes leading to the formation of

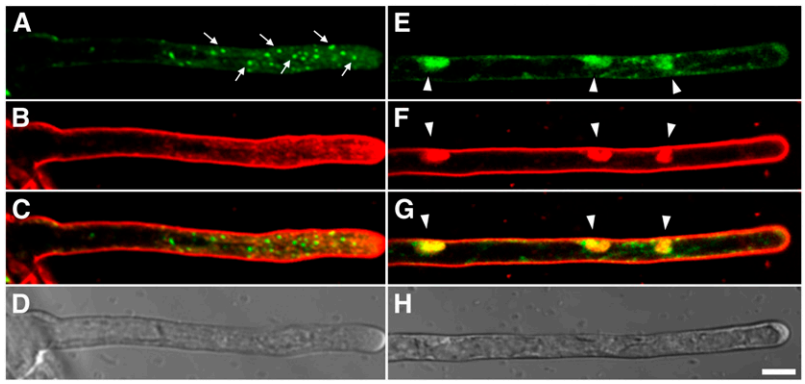

Figure 5. NHX5 Localizes to Punctate, Highly Motile Endosomal Bodies in Elongating in Root Hair Cells.

(A) and **(E)** Root hairs of the NHX5-YFP reporter are shown in green.
(B) and **(F)** Costaining with 4 μM FM4-64 (10 min).
(C) and **(G)** Overlay of NHX5-YFP and FM4-64.
(D) and **(H)** Respective differential interference contrast images of the same root hair cells shown in **(A)** to **(C)** and **(E)** to **(G)**.
(A) to **(D)** Untreated root hair.
(E) to **(H)** Root hair cell imaged after 30 min of 25 μM BFA treatment.
Arrows point to NHX5 positive motile endosomal bodies. Arrowheads point to BFA-induced agglomerations (so-called BFA compartments) of NHX5 and FM4-64–labeled endosomes. Bar = 10 μm. A time-lapse movie indicating the motile nature of NHX5 positive bodies can be found in Supplemental Movie 3 online.

BFA compartments were probably not affected significantly in *nhx5 nhx6.*

The delay in labeling of the tonoplast with FM4-64 prompted us to ask whether real vacuolar cargo, such as carboxypeptidase (CPY), might be missorted in *nhx5 nhx6* (Yamaguchi et al., 2003). We investigated possible missorting to the vacuole using yeast carboxypeptidase fused to GFP in transiently transformed seedlings. In cotyledons of wild-type seedlings, fluorescence was evident within mesophyll (Figure 7G) and epidermal cells (see Supplemental Figure 9A online) and was coincident with chloroplast localization. In *nhx5 nhx6*, however, GFP fluorescence was not detected within cells, as evidenced by the presence of chloroplasts, but rather in the apoplastic space surrounding individual mesophyll (Figure 7H) or epidermal cells (see Supplemental Figure 9B online). These data suggest that CPY is missorted to the apoplast in *nhx5 nhx6.*

Transcriptional Profiling of *nhx5* and *nhx6* Knockouts Implicate Roles in Stress Response

To investigate possible functions of *NHX5* and *NHX6*, we compared the expression profiles of two single knockouts (*nhx5-2* and *nhx6-2*), the two independently generated double knockout lines *nhx5-1 nhx6-1* (F-27) and *nhx5-2 nhx6-2* (F-37), and the wild type using the Affymetrix ATH1 genome array platform (see Methods for details on transcript analysis). The analysis of expressed transcripts in the five genotypes generated the expression profile shown in Figure 8. Within main clusters of gene expression, striking similarities between the wild type and the single knockouts and marked differences between the two *nhx5 nhx6* lines and the wild type, *nhx5*, and *nhx6* existed (Figure 8A). The two double knockout lines had highly similar expression patterns and differed by only 28 transcripts showing a significant fold change larger than $\log_2$ 0.5. Similarly, only nine transcripts were significantly different between *nhx5* and *nhx6*. The number of transcripts that were differentially expressed between *nhx5* and the wild type and *nhx6* and the wild type were 89 and 205, respectively.

Given the similarities in gene expression between single knockouts and the wild type (as well as their phenotypes), we proceeded to analyze transcripts that differed significantly between the double knockout *nhx5-2 nhx6-2* (F-37) and the wild type. Analysis of variance revealed 1728 transcripts that were differentially expressed in the double knockout compared with the wild type. Of those, 1079 transcripts were downregulated and 649 were upregulated in *nhx5 nhx6*. A short list of the most significantly changed transcripts ($\log_2$ fold change > 1.5) is included in Supplemental Table 1 online.

To infer biological function of differentially expressed transcripts in *nhx5 nhx6*, we performed an enrichment analysis of Gene Ontology (GO) terms (Brady et al., 2007). Data revealed a number of significantly enriched GO terms in both the up- and downregulated genes. A table including both up- and downregulated GO terms is included as Supplemental Table 2 online. We focused on two major functional groups of transcripts (Figures 8B and 8C). A number of GO categories related to stress responses, including response to abscisic acid (ABA) stimulus, desiccation, and salt stress, were among the most enriched. Transcripts associated with ABA responses were particularly enriched in *nhx5 nhx6*, including the upregulation of ABA receptors (RCAR 8, 10, and 12) and a downregulation of other ABA signaling components, such as ABI1, ABI2, HAB1, GPA1, and PLDα, among others (Figure 8C). The representation and large expression fold change of ABA-related genes suggest

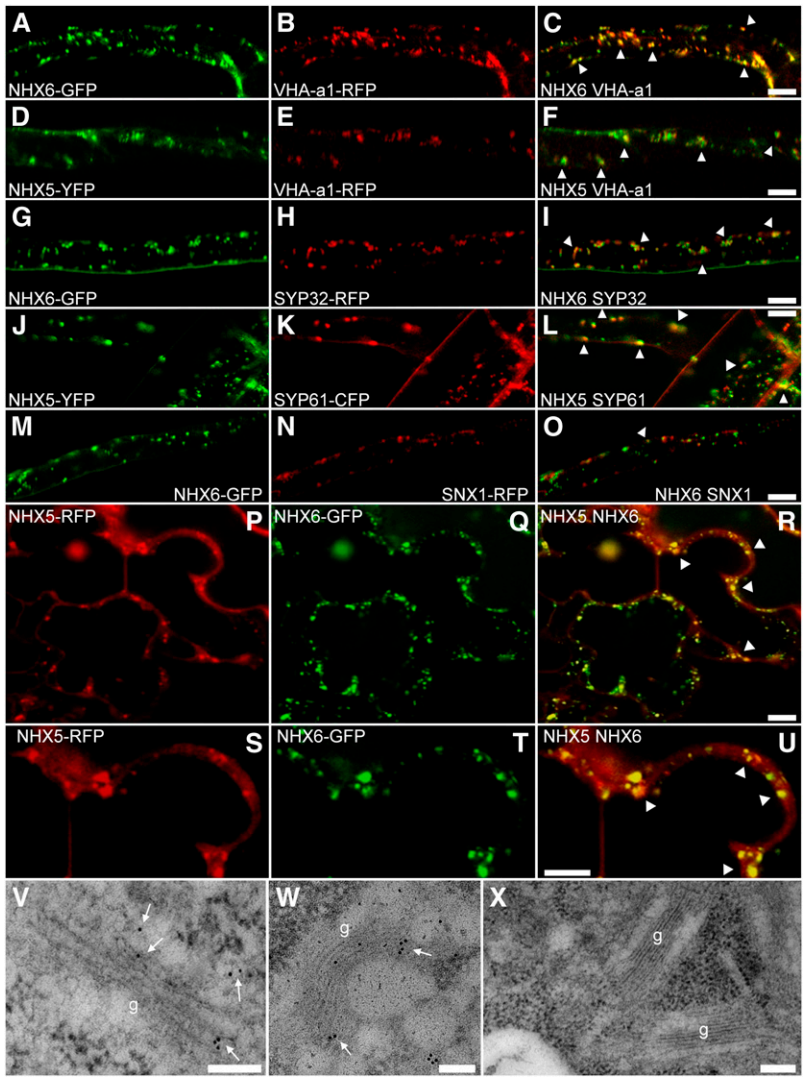

Figure 6. Colocalization of NHX5 and NHX6 with Endosomal Markers and Localization to Subcellular Compartments.

Images are confocal scans of double reporter lines coexpressing the following.
(A) to **(C)** NHX6-GFP and VHA-a1-RFP.
(D) to **(F)** NHX5-YFP and VHA-a1-RFP.
(G) to **(I)** NHX6-GFP and SYP32-RFP.
(J) to **(L)** NHX5-YFP and SYP61-CFP.
(M) to **(O)** NHX6-GFP and SNX1-RFP.
(P) to **(U)** Colocalization of NHX5-RFP and NHX6-GFP **(R)** in cotyledon epidermal cells of NHX6-GFP seedlings (shown in **[Q]** and **[T]**) transiently expressing NHX5-RFP (shown in **[P]** and **[S]**). **(S)** to **(U)** are close-ups of a region in **(P)** to **(R)** respectively.
Single-channel images are NHX6-GFP (**[A]**, **[G]**, **[M]**, **[Q]**, and **[T]**), NHX5-YFP (**[D]**, **[J]**, **[P]**, and **[S]**), VHA-a1-RFP (**[B]** and **[E]**), SYP32-RFP **(H)**, SYP61-CFP **(K)**, and SNX1-RFP **(N)**. The extent of colocalization (highlighted by arrowheads) is visible from overlays (**[C]**, **[F]**, **[I]**, **[L]**, **[O]**, **[R]**, and **[U]**).
(V) to **(X)** Immunogold localization of NHX6-GFP to the Golgi (g) and budding vesicles of the TGN (arrows) using anti-GFP antibody.
(X) Control labeling of wild-type seedlings was negligible.
Bars = 10 μm in **(A)** to **(O)**, 15 μm in **(P)** to **(U)**, and 50 nm in **(V)** to **(X)**.

a strong link to NHX5 and NHX6 functions. Another class of transcripts showing significantly altered expression in *nhx5 nhx6* included genes known to have roles in vesicular trafficking (Figure 8B). These included members of the RAB and ARF GTPase family (Rab5 members RABF2 and RAB3Ge), SNARE proteins (VTI12 and NPSN12), as well as vacuolar sorting receptors (VPS35, VPS20, and VSR1), among others (Figure 8B). The expression of all transcripts discussed above and shown in Figures 8B and 8C has been verified with qPCR in all of the five genotypes that were examined. Genes belonging to the GO

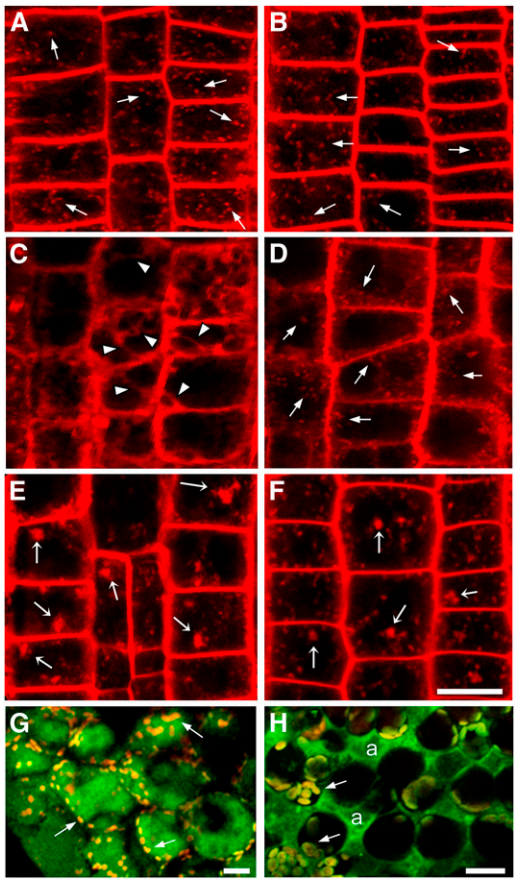

Figure 7. Trafficking to the Vacuole Is Affected in the *nhx5 nhx6* Double Knockout.

Roots of wild-type and *nhx5 nhx6* seedlings were stained with 4 μM FM4-64 as described in Methods. The progression of endomembrane staining was monitored in root tip cells over time. Arrows in **(A)**, **(B)**, and **(D)** indicate FM4-64–positive endocytosed bodies. Arrows in **(G)** and **(H)** point to chloroplasts. Bars = 10 μm in **(A)** to **(F)** and 25 μm in **(G)** and **(H)**.
(A) and **(B)** Root tip cells after 15 min of FM4-64 addition. The wild type **(A)** and *nhx5 nhx6* **(B)**.
(C) Wild-type root tip cells after 75 min of FM4-64 addition showing labeling of vacuolar membranes (arrow heads).
(D) *nhx5 nhx6* root tip cells after 95 min of FM4-64 addition. Note lack of staining of the tonoplast.
(E) and **(F)** Formation of so-called BFA bodies in the wild type **(E)** and *nhx5 nhx6* root tip cells **(F)** (arrows). Seedlings were treated with 25 μM BFA for 1 h before staining with FM4-64. Images shown were taken 15 min **(E)** and 30 min **(F)** after FM4-64 addition.
(G) and **(H)** Seedlings transiently expressing CPY-GFP in mesophyll cells of wild-type **(G)** or *nhx5 nhx6* **(H)** cotyledons. Note GFP fluorescence inside cells in **(G)** and in apoplast (a) in **(H)**. Arrows in **(G)** and **(H)** point to chloroplasts.

terms "structural constituent of the ribosome," "translation," and "ribosome biogenesis" were also downregulated, suggesting that protein translation may be restricted in *nhx5 nhx6* (see Supplemental Table 2 online). Interestingly, many cell wall–related transcripts were also significantly downregulated, especially those associated with structural proteins (arabinogalactans and facsilins), cell wall–modifying enzymes (expansins, xyloglucan endotransglycosylase, and hydrolases), as well as cell wall–degrading enzymes (polygalacturonase) (see Supplemental Table 2 online).

DISCUSSION

NHX5 and NHX6 Are Functionally Redundant and Play Key Roles in Cell Proliferation and Cell Growth

We used a reverse genetic approach to generate single and double knockouts of *NHX5* and *NHX6.* Single *nhx5* or *nhx6* knockouts did not exhibit any obvious growth phenotypes and closely resembled wild-type plants. Furthermore, transformation of *nhx5 nhx6* with either *NHX5* or *NHX6* rescued the *nhx5 nhx6* phenotype.

Gene expression patterns further supported the observed growth phenotypes of the knockouts. Gene expression in *nhx5* and *nhx6* were not only highly similar among each other but also similar to the wild type. Based on our phenotypic analysis of knockout and rescued lines, as well as gene expression patterns in single and double knockout lines, we conclude that *NHX5* and *NHX6* are functionally redundant. Nevertheless, the possibility that either *NHX5* or *NHX6* may have yet unknown specific roles remains open and cannot be excluded without further investigation.

Unlike single *nhx* knockouts, the double knockout *nhx5 nhx6* displayed drastically reduced growth and severely delayed development compared with wild-type plants. This phenotype was evident throughout development, from germination to flowering. Smaller growth in *nhx5 nhx6* was due mostly to a smaller cell size and slowed cell proliferation. Our data strongly suggest that *NHX5* and *NHX6* have fundamental roles necessary for cell expansion and cell proliferation rather than specific roles in cell identity or differentiation. Live-cell imaging of growing root hairs enabled the monitoring and quantification of growth at the single-cell level and indicated that *nhx5 nhx6* had one-third the rate of tip growth of wild-type cells in addition to a possible partial loss of tip-directed cytoplasmic streaming. Given the known dependence of growing root hairs on profuse and polar vesicular trafficking (Samaj et al., 2006), it is possible that trafficking of vesicular cargo or the cargo itself may be affected in *nhx5 nhx6*. Current data support that defects in vesicular trafficking might be a primary cause of the *nhx5 nhx6* phenotype (discussed below).

NHX5 and NHX6 Localize to the Golgi and TGN

Fluorescent protein fusion assays and immunogold labeling experiments indicated that both NHX5 and NHX6 are associated with highly motile, punctate endosomal bodies. Both NHX5 and NHX6 colocalized with the Golgi syntaxin SYP32 (Geldner et al., 2009) and the TGN markers VHA-a1 (Dettmer et al., 2006) and SYP61 (Robert et al., 2008), but not with the PVC marker SNX1 (Jaillais et al., 2008). Also, BFA caused the aggregation of NHX5- and NHX6-positive bodies into BFA compartments, further supporting a TGN or endosomal localization of both antiporters. Furthermore, the differential response of NHX6 VHA-a1 and

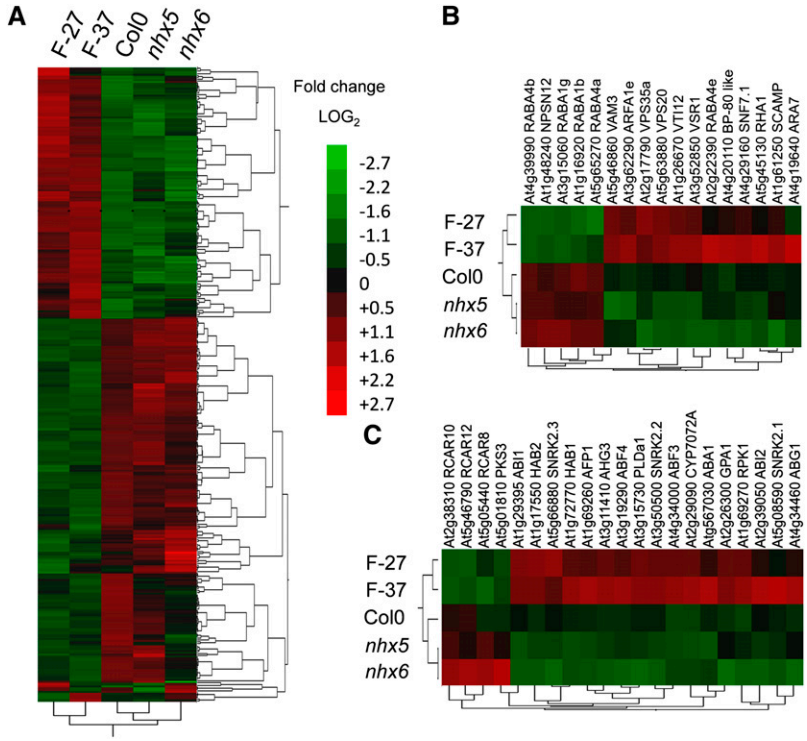

Figure 8. Transcriptional Profile of Single and Double Knockout Lines of *NHX5* and *NHX6*.

(A) Heat map of all genes with significantly altered expression
(B) Transcripts associated with vesicular trafficking
(C) Transcripts involved in ABA related responses
F-27 and F-37 are the double knockouts *nhx5-1 nhx6-1* and *nhx5-2 nhx6-2*, respectively. Upregulated genes are represented in red, while downregulated genes are represented in green. Expression is $\log_2$ transformed. Genes are clustered according to expression. Details of the transcriptional analysis are described in Methods.

NHX6 SYP32 to BFA indicated that NHX5 and NHX6 may exist in overlapping compartments (i.e., both TGN and Golgi). These results are in agreement with the known differential response of other Golgi and TGN proteins to BFA (Robinson et al., 2008). Our data confirm earlier predictions that suggested that NHX5 and NHX6 are localized to endosomal compartments similar to other homologs (Brett et al., 2005a; Pardo et al., 2006; Orlowski and Grinstein, 2007; Rodríguez-Rosales et al., 2009). The localization of NHX5 and NHX6 was assessed using C-terminal GFP/YFP tagging; therefore, it is possible that the localization to the Golgi/TGN may have been influenced by the presence of the tag. Tagging of NHX5 and NHX6 in other parts of the proteins is needed to confirm any effect of terminal tagging on localization. Nevertheless, the recovery of the wild-type phenotype when either *NHX5-YFP* or *NHX6-GFP* was expressed in the double knockout *nhx5 nhx6* would argue against a possible interference of C-terminal tagging with protein localization.

The TGN has emerged as an important sorting organelle where secretory and endocytotic trafficking pathways converge (Dettmer et al., 2006; Lam et al., 2009; Viotti et al., 2010). In plants, localization of NHX5 and NHX6 to the TGN suggests several possible functional roles for endosomal Na^+/H^+ antiporters that are likely to be distinct from other vacuolar NHX isoforms. Nonfunctional TGN may cause missorting of vesicles containing proteins, membrane, and cell wall components that are necessary for cell expansion. Alternatively, given the localization of NHX5 and NHX6 to the Golgi, vesicular cargo itself may be affected due to defects in the posttranslational modification of proteins and/or synthesis of cell wall polysaccharides. The latter is supported by microarray data in which transcripts of a number of cell wall–related enzymes (e.g., xyloglucan endotransglycosylase) were significantly upregulated in *nhx5 nhx6*.

NHX5 and NHX6 Mediate Vesicular Trafficking

In *nhx5 nhx6* root tip cells, endocytosis was not significantly affected because early endosomal bodies were observed after FM4-64 application, similar to wild-type cells. Furthermore, pretreatment of *nhx5 nhx6* root tip cells with BFA caused the expected formation of BFA compartments (containing FM4-64). Together, these data indicate that early endocytotic steps were probably not affected in *nhx5 nhx6.* Instead, we noted that in *nhx5 nhx6*, the labeling of vacuoles with FM4-64 was either severely inhibited or delayed. In addition to the delay in FM4-64

trafficking to the vacuole, we also noted a missorting of CPY to the apoplast. Missorting of vacuole-destined cargo is a common feature of several trafficking mutants (Fuji et al., 2007; Craddock et al., 2008; Zouhar et al., 2009). These data implicate NHX5 and NHX6 in roles at the TGN, Golgi, or related endosomal compartments that either regulate or act as intermediates of cellular cargo destined to the vacuole.

Transcriptional analysis identified a number of trafficking-related transcripts with significantly altered expression in *nhx5 nhx6*, including *VTI12*, *VSR1*, *RABF2a*, *VPS35*, and *ARFa1e*, among others. The SNARE VTI12 forms a complex with SYP41 SYP61 VPS45 at the TGN (Zouhar et al., 2009) that regulates trafficking of storage proteins to vacuoles (Sanmartín et al., 2007). RNA interference silencing of VPS45, an *Arabidopsis* homolog of yeast Sec1, caused defects in vacuole formation, mistargeting of vacuolar proteins, and a dwarf phenotype due to small cell size (Zouhar et al., 2009). Similar phenotypes were also noted for VPS35 knockouts, a PVC retromer component with roles in storage protein trafficking (Yamazaki et al., 2008). The Rab5 members, RABF2a (Rha1) and RABF2b (Ara7), localize to the PVC and are implicated in transport to vacuoles and in endocytosis (Sohn et al., 2003; Kotzer et al., 2004). Interestingly, antisense ARF1 plants (the endosomal GTPase implicated in vesicular transport) had smaller cells and a slower rate of cell proliferation resulting in small plants (Gebbie et al., 2005; Xu and Scheres, 2005). The phenotypic similarity of *nxh5 nhx6* to *ARF1* antisense plants and *vps* mutants is striking and strongly supports roles of NHX5 and NHX6 in trafficking to the vacuole.

Endosomal NHXs Are Necessary to Mediate the Response of *Arabidopsis* to Salt Stress

The *nhx5 nhx6* knockout exhibited extreme sensitivity to salinity, especially at germination. The importance of endosomal NHXs in salt tolerance has been demonstrated in close homologs of NHX5 and NHX6. *Nhx1Δ* yeast mutants are similarly sensitive to salt stress (Nass et al., 1997). Silencing of NHX2 in tomato also led to an inhibition of plant growth as well as increased sensitivity to salt (Rodriguez-Rosales et al., 2008). Given NHX5 and NHX6 localization and the observed defects in vacuolar trafficking in *nhx5 nhx6*, it is possible that missorting of vacuolar transporters, needed for salt sequestration, may be a cause of the high sensitivity to salt. Endosomal trafficking, and especially vesicle fusion to the vacuole, is increasingly considered an important component of cellular responses to stresses such as high salt and reactive oxygen species (Mazel et al., 2004; Leshem et al., 2006; Hamaji et al., 2009). Additional tonoplast transporters with roles in Na^+ sequestration, such as NHX1 (Apse et al., 1999), primary pumps (Gaxiola et al., 2001), and water channels (Sade et al., 2010), also depend on vesicular trafficking for their delivery to the tonoplast. It is therefore possible that NHX5 and NHX6 may affect protein trafficking from the Golgi/TGN to vacuoles, necessary for response to high salt. The importance of excluding deleterious cations, such as Na^+, from accumulating in endosomes/PVC was also recently highlighted (Hernández et al., 2009). The upregulation of *NHX5* transcripts in response to salt, but not osmotic shock, supports a role for *NHX5*/*NHX6* in the response to salt (Yokoi et al., 2002).

Possible Functions of NHX5 and NHX6

The molecular basis for the trafficking defects we observe is probably linked to K^+ and/or pH homeostasis of endosomal compartments. Little is known about the roles of K^+ in endosomal processes, but in yeast, Kex2/furin endoproteases require K^+ as a cofactor for the maturation of newly synthesized proteins of the secretory pathway (Rockwell and Fuller, 2002). pH regulation, however, is a well-known factor affecting endosomal protein processing and trafficking. Organelles of the secretory and endocytotic pathway have unique luminal pHs, generated by endosomal V-ATPases, as shown in animal systems (Marshansky and Futai, 2008). Increasing acidity of endocytotic bodies correlates with maturation and is a requisite for their delivery to lysosomes (vacuoles). Similarly, anterograde vesicles also have progressively decreasing pH (i.e., endoplasmic reticulum = 7.0; TGN = 6.5; apoplast = 5.5) that is critical for posttranslational processing and sorting of newly synthesized material. It appears that this is highly conserved across taxa. In humans, NHE isoforms are distributed in discrete compartments of the endomembrane system (Orlowski and Grinstein, 2007). Endosomal NHXs may provide the H^+ leak necessary to counter luminal acidification generated by the V-ATPase and thus enable the maintenance of organelle-specific luminal pH (Orlowski and Grinstein, 2007), with important implications to processing and sorting of cellular cargo.

Colocalization of NHX5 and NHX6 with VHA-a1 supports a possible functional relationship between the antiporters and the H^+-pump. Reduced activity of the TGN VHA-a1 isoform caused a cessation in cell expansion (Brüx et al., 2008), and the V-ATPase inhibitor Concanamycin A blocked endocytotic transport of FM4-64 to the vacuole (Dettmer et al., 2006). Increased salt sensitivity was also observed in the knockdown of the TGN/EE V-ATPase isoform (Brüx et al., 2008). A null mutant of the yeast homolog Nhx1 (*nhx1Δ*) displayed aberrant accumulation and processing of vacuolar-targeted proteins (Bowers et al., 2000; Ali et al., 2004), which was linked to an observed acidification of endosomes in *nhx1Δ* because weak base alleviated the protein trafficking defects in *nhx1Δ* (Brett et al., 2005b). We expect that endosomal pH may be similarly affected in *nhx5 nhx6*, and efforts are currently under way to measure endosomal pH. Overexpression of human NHE9, which is localized to late recycling endosomes, caused an increased the luminal pH of compartments in which the proteins were localized, from mildly acidic pH to cytosolic pH, suggesting that their in vivo function is to regulate the pH and cation concentration (Nakamura et al., 2005). It was recently shown that a pH-dependent interaction of vesicles with Arf GTPase, ARNO (GDP/GTP exchange factor), and coat proteins occurs and that V-ATPase acts as a scaffold to recruit Arf6 in a pH-dependent manner that is crucial to trafficking between early and late endosomes (Hurtado-Lorenzo et al., 2006). Interestingly, a SCAMP that was shown to bind to Arf6 and PLD1, and is also involved in the redistribution of NHE7 from recycling endosomes to the TGN (Lin et al., 2005), was significantly upregulated in *nhx5 nhx6*. These findings raise the interesting possibility that a SCAMP, Arf6, and NHE7 may form a macromolecular complex that functionally links endosomal acidification (V-ATPase), a NHE/NHX alkalinizing mechanism, and protein trafficking. Collectively,

these data would support the notion that NHX5 and NHX6 might regulate endosomal pH and K^+ (Na^+) homeostasis, which in turn affects intracellular endosomal transport.

In conclusion, we demonstrated that normal growth and development, as well as response to stress, require NHX5 and NHX6 and that the two proteins are functionally redundant. Unlike other *Arabidopsis* NHX isoforms, which are vacuolar, our results show that NHX5 and NHX6 are localized to endosomal compartments associated with the TGN and Golgi. Our data highlight the importance of endosomal NHX antiporters in plants and raise interesting questions on roles of NHX in protein processing and trafficking of intracellular cargo.

METHODS

Plant Materials and Growth Conditions

Arabidopsis thaliana (ecotype Columbia [Col-0]) was grown at 22°C under diurnal light conditions (16 h light and 8 h dark) unless specified otherwise. For plate-grown plants, modified Murashige and Skoog media (Spalding et al., 1999) was used and complemented with 1% Phytagel (Sigma-Aldrich), without sucrose. pH was adjusted to 5.7 with 1 M NaOH and supplemented with 1 M NaCl to make final concentration of 1 mM Na^+. For salinity stress on plates, NaCl was added to the basal growth media to final concentrations as indicated in the figure legends. Plates were incubated at 22°C under 12 h light and 12 h dark.

T-DNA insertion mutants (Col ecotype) (http://signal.salk.edu/cgi-bin/tdnaexpress; http://www.gabi-kat.de/) for NHX5 were *nhx5-1* (WiscDsLox345-348M8) and *nhx5-2* (GABI_094H05) and for NHX6 were *nhx6-1* (SALK_113129) and *nhx6-2* (SALK_100042). Positions of T-DNA insertion sites are shown in Supplemental Figure 3A online. Additional T-DNA knockouts were *nhx1-2* (SALK_065623) for NHX1 and *nhx3-1* for NHX3 (WiscDsLox345-348F19). RT-PCR analyses confirmed no or very low DNA amplification with allele-specific primers from knockout-derived cDNA. All single knockouts were backcrossed with Col wild-type plants at least twice, and corresponding lines with single T-DNA insertions were selected by DNA gel blot hybridization using the left border sequence as the probe. Primer sequences for the confirmation of homozygous T-DNA insertions are listed in Supplemental Table 3 online. Seeds expressing AtVHA-a1-RFP were a gift from Karin Schumacher (Dettmer et al., 2006); AtSYP61-RFP seeds were a gift from Natasha Raikhel (Robert et al., 2008); AtSNX1-RFP seeds were a gift from Thierry Gaude (Jaillais et al., 2008); and AtSYP32-RFP seeds were obtained from the Nottingham Arabidopsis Stock Centre (Geldner et al., 2009). To generate double reporter lines coexpressing VHA-a1, SYP61, SNX1, or SYP32 with either NHX5-YFP or NHX6-GFP, homozygous parents were crossed using NHX5-YFP or NHX6-GFP as pollen donors. The resulting F1 seedlings were used for fluorescence microscopy (see below).

RNA Preparation and Expression Analysis

Total RNA was extracted from rosette leaves using the RNeasy Mini kit (Qiagen) with six biological replicates, treated with DNaseI and subsequently purified with RNeasy RNA purification column (Qiagen). First-strand cDNA was synthesized from 1 μg of total RNA with the QuantiTect reverse transcription kit (Qiagen). Primer Express (Applied Biosystems Life Technologies) was used to design primers. qPCR was performed on the StepOnePlus (Applied Biosystems) using SYBR GREEN (Bio-Rad). The reaction volume included 2 μL of template, 0.3 μL of reverse primer, 0.3 μL of forward primer, 7.5 μL of 2X SYBR Green Master Mix, and 4.9 μL of RNA-free water (total 15 μL). qPCR was performed as follows: 95°C for 10 min follow by 40 cycles of 95°C for 30 s and 60°C for 30 s. The 2-ΔΔCT method (Livak and Schmittgen, 2001) was used to determine the relative mRNA using *PP2A* as an internal reference. Reference genes were previously found to express similarly in all genotypes and organs examined here. Primer sequences for RT-PCR and qPCR are listed in Supplemental Table 3 online.

Plasmid Construction and Plant Transformation

NHX5-YFP and *NHX6-GFP* were constructed using Gateway technology (Invitrogen). cDNAs from NHX5 and NHX6 (without stop codons) were cloned into pDONR207 (Invitrogen) and recombined into pEarleyGate101 for YFP fusion and pEarleyGate103 for GFP fusion (Earley et al., 2006). The constructs were introduced into *Arabidopsis* Col-0 plants expressing translational fusion proteins and into *nhx5-2 nhx6-2* for complementation by *Agrobacterium tumefaciens* (GV3101) using the floral dipping method (Clough and Bent, 1998). For CPY-GFP, an N-terminal part of *Saccharomyces cerevisiae* CPY was fused with GFP by PCR and cloned into pDONR207. Fusion cDNA of CPY and GFP was recombined into pEarleyGate 100. Transient expression in cotyledons of *Arabidopsis* seedlings was performed according to Marion et al. (2008). Seedlings were kept in the dark until observation. A list of primers is included in Supplemental Table 3 online.

Histological Analysis

Plant tissues were trimmed, immediately fixed in FAA (formalin, acetic acid, and alcohol), vacuum infiltrated for 30 min, and left at 4°C overnight. Tissues were then rinsed three times with 70% ethanol and dehydrated in a graded ethanol series (70, 85, 95, and 2× 100%). Xylenes were gradually incorporated into the tissues (1:3, 1:1, 3:1, and 2× 100%) before paraffin chips were added to the vials and kept on a rotary shaker overnight at room temperature. Vials were then incubated at 42°C for at least 1 h before being transferred to a 60°C oven. The xylene/paraffin mixture was then replaced with 100% paraffin. Tissues were infiltrated with molten paraffin for 3 d at 60°C before being mounted and sectioned. Five-micrometer-thick serial sections were cut using a Leica RM2125RT rotary microtome (Leica Microsystems). Slides were dried at room temperature and deparaffinized in 2× 100% xylene for 2 min before use in histological studies. Serial sections were stained with periodic acid–Schiff for total carbohydrates and counterstained with amido black 10B for protein or toluidine blue O for general histological organization (Yeung, 1999).

Chemical Treatment of Seedlings

Whole seedlings (4 d old grown on vertical plates) were mounted vertically in liquid medium between slide and cover slip, separated by a Parafilm strip spacer, and allowed to adjust in a humid glass chamber under standard growth conditions for at least 12 h before observation. Liquid culture medium had the same composition as plates but without Phytagel. Only seedlings exhibiting abundant root hair growth were selected for subsequent experiments and observations of roots and root hair cells. Seedlings were treated while on slides and under microscopy observation by perfusing medium containing treatment chemicals with the aid of a piece of filter paper to pull solution from one end of the slide while applying new medium at the other end. All dye and inhibitor treatments were performed in this way. BFA was applied at 25 μM in culture medium. For endocytosis and colocalization, roots were stained with 4 μM FM4-64 for 5 min and washed.

Fluorescence and Light Microscopy

Fluorescence microscopy was performed using a Leica confocal laser scanning microscope (DM RXE 6 TCS-SP2 AOBS) equipped with a ×63

water immersion objective. The excitation wavelength was 488 nm, and emission for GFP was 500 to 535 nm, for RFP was 565 to 605 nm, and for FM4-64 was 620 to 670 nm. For multicolor imaging of GFP/RFP, CFP/YFP, and YFP/RFP double reporter lines, sequential scanning was used to avoid crosstalk between fluorescence channels. Images were processed with ImageJ (http://rsbweb.nih.gov/ij/). Quantification of colocalization was performed using the intensity correlation analysis plug-in of the MBF ImageJ bundle according to Li et al. (2004). This analysis delivers a coefficient, ranging from 0 for no colocalization to 0.5 for high colocalization. Growth of root hair cells was estimated by tracking the extension of root hair tips in a sequence (stack) of acquired images using the Track Objects function of MetaMorph (Molecular Devices).

Electron Microscopy and Immunolocalization

Five-day-old seedlings grown on vertical plates were chemically fixed in 4% paraformaldehyde in 0.1 M phosphate buffer under vacuum (1 h) with microwave assistance. Tissue was dehydrated and infiltrated with LR White as outlined previously (Shipman and Inoue, 2009). Immunolabeling was performed on ultrathin sections collected on Formvar-coated grids using rabbit anti-GFP (1:200; Novus Biologicals) and goat anti-rabbit with 10-nm gold (1:50; BioCell International). Grids were stained with uranyl acetate and lead citrate before viewing on a Phillips CM120 Biotwin (FEI) at the University of California, Davis (Electron Microscopy Laboratory, Department of Pathology and Laboratory Medicine, School of Medicine).

Microarray Analysis

Mature rosette leaves from 20 soil-grown plants of the wild type, *nhx5-2*, *nhx6-2*, *nhx5-1 nhx6-1* (F-37), and *nhx5-2 nhx6-2* (F-27) were pooled for RNA extraction (RNeasy Mini kit; Qiagen) into each of three replicates per genotype. Residual DNA was removed with in-column *DNaseI* digestion. The quality of RNA was determined using the Nanodrop ND-1000. Two micrograms of total RNA from each genotype was used to generate labeled amplified RNA using the GeneChip 3′ IVT Express Kit package (Affymetrix) and used to hybridize to the Affymetrix GeneChip following the manufacturer's instructions. Washing and staining steps were performed using the GeneChip Fluidics Station 450. Arrays were scanned with the GeneChip Scanner 3000 7G piloted by the Affymetrix GeneChip operating software. GeneChip images were examined for visual aberrations before performing normalization and statistical analysis (JMP Genomics 3.2; SAS Institute). Probe intensity signal values were transformed to $\log_2$ scale and background normalized. A quality control procedure was used to assess the hybridization quality between and within arrays. To evaluate data quality, we first tested the distribution of row data followed by principle component analysis. Because of the high quality of the arrays, we performed mild data normalization using the standard deviation procedure (SAS Institute) and reevaluated data quality after normalization. In addition, we compared the output resulting from quantile normalization and found that these did not differ significantly from outputs obtained using the standard deviation procedure. Analysis of variance was used to test differentially expressed transcripts between the five genotypes (G). In the analysis of variance model, G and probe were considered as fixed effects and array as a random effect. The threshold of significance was based on a Bonferroni correction of $P = 0.05$ (Hochberg, 1988). Because Bonferroni correction yielded a gene expression comparison that was highly significant, only fold change was used as a criterion for discussing differences in transcript expression. We also compared subsets of genotypes using the same statistical procedure. Two-way hierarchal clustering analysis was performed using normalized probe set expression values. Probe sets were clustered according to expression patterns, with distances between clusters defined by the Ward method (SAS Institute).

Microarray data was processed using the ChipEnrich software, which uses the Apache Commons Math library to calculate P values based on hypergeometric distribution as described (Brady et al., 2007; Orlando et al., 2009). This program can test for enrichment of GO terms (TAIR9; August, 2009) based on singletons that map to a single Arabidopsis Genome Initiative locus identifier on the ATHI GeneChip. Enrichment of GO categories was analyzed as described by Brady et al. (2007). GO annotations were downloaded from The Arabidopsis Information Resource (TAIR9; October, 2009). When analyzing the data, parent-child relationships were not considered. GO categories were considered statistically enriched within a given coexpression gene list if a P value was < 0.001.

Phylogenetic Analysis

Phylogenic analysis was performed using the DNASIS sequence analysis software (http://www.miraibio.com/dnasis-max/dnasis-max-overview.html) with automatic multiple alignment settings. Parameters for "gap penalty, K-tuple, number of top diagonals, window size, fixed gap penalty and floating gap penalty" were 5, 2, 5, 12, 10, and 10, respectively. Bootstrap values from at least 1000 trials were used.

Accession Numbers

Sequence data from this article can be found in the Arabidopsis Genome Initiative database under the following accession numbers: NHX5 (At1g54370), NHX6 (At1g79610), NHX1 (At5g27150), NHX3 (At5g55470), VHA-a1 (At2g28520), SYP61 (At1g28490), SNX1 (At5g06140), and SYP32 (At3g24350). CEL files of all 15 Affymetrix GeneChips from this study were deposited in the public microarray database at the National Center for Biotechnology Information Gene Expression Omnibus (https://www.ncbi.nlm.nih.gov/projects/geo) under accession number GSE23210.

Supplemental Data

The following materials are available in the online version of this article.

Supplemental Figure 1. Phylogeny and Sequence Alignment of the *Arabidopsis* Intracellular NHX Proteins (see Supplemental Data Set 1 online).

Supplemental Figure 2. Tissue-Specific Expression of *NHX5* and *NHX6.*

Supplemental Figure 3. T-DNA Insertion Mutants of *NHX5* and *NHX6.*

Supplemental Figure 4. Root Phenotype of the Double Knockout *nhx5 nhx6.*

Supplemental Figure 5. Rescue of the *nhx5 nhx6* Double Knockout.

Supplemental Figure 6. Phenotype of the Single Knockouts, *nhx5-2* and *nhx6-2*, and the double Knockouts, *nhx1 nhx5* and *nhx3 nhx5*, When Grown under Salt.

Supplemental Figure 7. Subcellular Localization of NHX5 and NHX6 in Different Organs and Cell Types.

Supplemental Figure 8. Response of Double Reporters NHX6-GFP VHA-a1-RFP and NHX6-GFP SYP32-RFP to Brefeldin A.

Supplemental Figure 9. Missorting of Carboxypeptidase in *nhx5 nhx6* Epidermal Cells.

Supplemental Table 1. List of Transcripts Showing the Highest Significant Fold Change between the Wild Type and *nhx5 nhx6.*

Supplemental Table 2. Changes in Most Significantly Enriched GO Categories.

Supplemental Table 3. List of Primers Used in This Study.

Supplemental Movie 1. Movie of Figure 3C.

Supplemental Movie 2. Cytoplasmic Streaming of Root Hair Cells in the Wild Type and the *nhx5 nhx6* Double Knockout.

Supplemental Movie 3. Movie of Figure 5A.

Supplemental Movie Legends.

Supplemental Data Set 1. Text File of the Alignment Used for the Phylogenetic Analysis Shown in Supplemental Figure 1A.

ACKNOWLEDGMENTS

We thank Natasha Raikhel for providing SYP61-CFP, Karin Schumacher for VHA-a1-RFP, and Thierry Gaude for SNX1-RFP plants. We also thank Ehud Katz, Georgia Drakakaki, Iana Kostina, and Ardian Coku for helpful discussions and technical assistance. This work was supported in part by grants from the National Science Foundation (MCB-0343279; IOS-0820112) and the Will W. Lester Endowment, University of California, to E.B. Z.P. was supported by the Vaadia-BARD postdoctoral Fellowship Award (FI-419-08) from the U.S.–Israel Binational Agricultural Research and Development Fund.

Received September 10, 2010; revised December 20, 2010; accepted January 3, 2011; published January 28, 2011.

REFERENCES

Aharon, G.S., Apse, M.P., Duan, S., Hua, X., and Blumwald, E. (2003). Characterization of a family of vacuolar Na+/H+ antiporters in *Arabidopsis thaliana.* Plant Soil **253:** 245–256.

Ali, R., Brett, C.L., Mukherjee, S., and Rao, R. (2004). Inhibition of sodium/proton exchange by a Rab-GTPase-activating protein regulates endosomal traffic in yeast. J. Biol. Chem. **279:** 4498–4506.

Apse, M.P., Aharon, G.S., Snedden, W.A., and Blumwald, E. (1999). Salt tolerance conferred by overexpression of a vacuolar Na^+/H^+ antiport in Arabidopsis. Science **285:** 1256–1258.

Apse, M.P., and Blumwald, E. (2007). Na+ transport in plants. FEBS Lett. **581:** 2247–2254.

Apse, M.P., Sottosanto, J.B., and Blumwald, E. (2003). Vacuolar cation/H+ exchange, ion homeostasis, and leaf development are altered in a T-DNA insertional mutant of AtNHX1, the Arabidopsis vacuolar Na+/H+ antiporter. Plant J. **36:** 229–239.

Bassham, D., Brandizzi, F., Otegui, M., and Sanderfoot, A. (September 30, 2008). The secretory system of Arabidopsis. In The Arabidopsis Book, C.R. Somerville and E.M. Meyerowitz, eds (Rockville, MD: American Society of Plant Biologists), doi/10.1199/tab.0116, http://www.aspb.org/publications/arabidopsis/.

Bowers, K., Levi, B.P., Patel, F.I., and Stevens, T.H. (2000). The sodium/proton exchanger Nhx1p is required for endosomal protein trafficking in the yeast *Saccharomyces cerevisiae*. Mol. Biol. Cell **11:** 4277–4294.

Brady, S.M., Orlando, D.A., Lee, J.-Y., Wang, J.Y., Koch, J., Dinneny, J.R., Mace, D., Ohler, U., and Benfey, P.N. (2007). A high-resolution root spatiotemporal map reveals dominant expression patterns. Science **318:** 801–806.

Brett, C.L., Donowitz, M., and Rao, R. (2005a). Evolutionary origins of eukaryotic sodium/proton exchangers. Am. J. Physiol. Cell Physiol. **288:** C223–C239.

Brett, C.L., Tukaye, D.N., Mukherjee, S., and Rao, R.J. (2005b). The yeast endosomal Na+K+/H+ exchanger Nhx1 regulates cellular pH to control vesicle trafficking. Mol. Biol. Cell **16:** 1396–1405.

Brüx, A., Liu, T.Y., Krebs, M., Stierhof, Y.D., Lohmann, J.U., Miersch, O., Wasternack, C., and Schumacher, K. (2008). Reduced V-ATPase activity in the trans-Golgi network causes oxylipin-dependent hypocotyl growth Inhibition in *Arabidopsis*. Plant Cell **20:** 1088–1100.

Clough, S.J., and Bent, A.F. (1998). Floral dip: A simplified method for Agrobacterium-mediated transformation of *Arabidopsis thaliana.* Plant J. **16:** 735–743.

Craddock, C.P., Hunter, P.R., Szakacs, E., Hinz, G., Robinson, D.G., and Frigerio, L. (2008). Lack of a vacuolar sorting receptor leads to non-specific missorting of soluble vacuolar proteins in Arabidopsis seeds. Traffic **9:** 408–416.

Dettmer, J., Hong-Hermesdorf, A., Stierhof, Y.D., and Schumacher, K. (2006). Vacuolar H+-ATPase activity is required for endocytic and secretory trafficking in *Arabidopsis*. Plant Cell **18:** 715–730.

Earley, K.W., Haag, J.R., Pontes, O., Opper, K., Juehne, T., Song, K., and Pikaard, C.S. (2006). Gateway-compatible vectors for plant functional genomics and proteomics. Plant J. **45:** 616–629.

Fuji, K., Shimada, T., Takahashi, H., Tamura, K., Koumoto, Y., Utsumi, S., Nishizawa, K., Maruyama, N., and Hara-Nishimura, I. (2007). Arabidopsis vacuolar sorting mutants (green fluorescent seed) can be identified efficiently by secretion of vacuole-targeted green fluorescent protein in their seeds. Plant Cell **19:** 597–609.

Gaxiola, R.A., Li, J.S., Undurraga, S., Dang, L.M., Allen, G.J., Alper, S.L., and Fink, G.R. (2001). Drought- and salt-tolerant plants result from overexpression of the AVP1 H+-pump. Proc. Natl. Acad. Sci. USA **98:** 11444–11449.

Gebbie, L.K., Burn, J.E., Hocart, C.H., and Williamson, R.E. (2005). Genes encoding ADP-ribosylation factors in *Arabidopsis thaliana* L. Heyn.: Genome analysis and antisense suppression. J. Exp. Bot. **56:** 1079–1091.

Geldner, N., Anders, N., Wolters, H., Keicher, J., Kornberger, W., Muller, P., Delbarre, A., Ueda, T., Nakano, A., and Jürgens, G. (2003). The Arabidopsis GNOM ARF-GEF mediates endosomal recycling, auxin transport, and auxin-dependent plant growth. Cell **112:** 219–230.

Geldner, N., Dénervaud-Tendon, V., Hyman, D.L., Mayer, U., Stierhof, Y.D., and Chory, J. (2009). Rapid, combinatorial analysis of membrane compartments in intact plants with a multicolor marker set. Plant J. **59:** 169–178.

Hamaji, K., et al. (2009). Dynamic aspects of ion accumulation by vesicle traffic under salt stress in Arabidopsis. Plant Cell Physiol. **50:** 2023–2033.

Hepler, P.K., Vidali, L., and Cheung, A.Y. (2001). Polarized cell growth in higher plants. Annu. Rev. Cell Dev. Biol. **17:** 159–187.

Hernández, A., Jiang, X.Y., Cubero, B., Nieto, P.M., Bressan, R.A., Hasegawa, P.M., and Pardo, J.M. (2009). Mutants of the *Arabidopsis thaliana* cation/H+ antiporter AtNHX1 conferring increased salt tolerance in yeast: The endosome/prevacuolar compartment is a target for salt toxicity. J. Biol. Chem. **284:** 14276–14285.

Hochberg, Y. (1988). A sharper Bonferroni procedure for multiple tests of significance. Biometrika **75:** 800–802.

Hurtado-Lorenzo, A., Skinner, M., El Annan, J., Futai, M., Sun-Wada, G.H., Bourgoin, S., Casanova, J., Wildeman, A., Bechoua, S., Ausiello, D.A., Brown, D., and Marshansky, V. (2006). V-ATPase interacts with ARNO and Arf6 in early endosomes and regulates the protein degradative pathway. Nat. Cell Biol. **8:** 124–136.

Jaillais, Y., Fobis-Loisy, I., Miège, C., and Gaude, T. (2008). Evidence for a sorting endosome in Arabidopsis root cells. Plant J. **53:** 237–247.

Kotzer, A.M., Brandizzi, F., Neumann, U., Paris, N., Moore, I., and Hawes, C. (2004). AtRabF2b (Ara7) acts on the vacuolar trafficking pathway in tobacco leaf epidermal cells. J. Cell Sci. **117:** 6377–6389.

Lam, S.K., Cai, Y., Tse, Y.C., Wang, J., Law, A.H.Y., Pimpl, P., Chan, H.Y.E., Xia, J., and Jiang, L. (2009). BFA-induced compartments from the Golgi apparatus and *trans*-Golgi network/early endosome are distinct in plant cells. Plant J. **60:** 865–881.

Leidi, E.O., Barragán, V., Rubio, L., El-Hamdaoui, A., Ruiz, M.T., Cubero, B., Fernández, J.A., Bressan, R.A., Hasegawa, P.M., Quintero, F.J., and Pardo, J.M. (2010). The AtNHX1 exchanger mediates potassium compartmentation in vacuoles of transgenic tomato. Plant J. **61:** 495–506.

Leshem, Y., Melamed-Book, N., Cagnac, O., Ronen, G., Nishri, Y., Solomon, M., Cohen, G., and Levine, A. (2006). Suppression of Arabidopsis vesicle-SNARE expression inhibited fusion of H2O2-containing vesicles with tonoplast and increased salt tolerance. Proc. Natl. Acad. Sci. USA **103:** 18008–18013.

Li, Q., Lau, A., Morris, T.J., Guo, L., Fordyce, C.B., and Stanley, E.F. (2004). A syntaxin 1, Galpha(o), and N-type calcium channel complex at a presynaptic nerve terminal: Analysis by quantitative immunocolocalization. J. Neurosci. **24:** 4070–4081.

Lin, P.J.C., Williams, W.P., Luu, Y., Molday, R.S., Orlowski, J., and Numata, M. (2005). Secretory carrier membrane proteins interact and regulate trafficking of the organellar (Na+,K+)/H+ exchanger NHE7. J. Cell Sci. **118:** 1885–1897.

Livak, K.J., and Schmittgen, T.D. (2001). Analysis of relative gene expression data using real-time quantitative PCR and the 2(T)(-Delta Delta C) method. Methods. **25:** 402–408.

Marion, J., Bach, L., Bellec, Y., Meyer, C., Gissot, L., and Faure, J.D. (2008). Systematic analysis of protein subcellular localization and interaction using high-throughput transient transformation of Arabidopsis seedlings. Plant J. **56:** 169–179.

Marshansky, V., and Futai, M. (2008). The V-type H+-ATPase in vesicular trafficking: Targeting, regulation and function. Curr. Opin. Cell Biol. **20:** 415–426.

Maser, P., et al. (2001). Phylogenetic relationships within cation transporter families of Arabidopsis. Plant Physiol. **126:** 1646–1667.

Mazel, A., Leshem, Y., Tiwari, B.S., and Levine, A. (2004). Induction of salt and osmotic stress tolerance by overexpression of an intracellular vesicle trafficking protein AtRab7 (AtRabG3e). Plant Physiol. **134:** 118–128.

Nakamura, N., Tanaka, S., Teko, Y., Mitsui, K., and Kanazawa, H. (2005). Four Na+/H+ exchanger isoforms are distributed to Golgi and post-Golgi compartments and are involved in organelle pH regulation. J. Biol. Chem. **280:** 1561–1572.

Nass, R., Cunningham, K.W., and Rao, R. (1997). Intracellular sequestration of sodium by a novel Na+/H+ exchanger in yeast is enhanced by mutations in the plasma membrane H+-ATPase. Insights into mechanisms of sodium tolerance. J. Biol. Chem. **272:** 26145–26152.

Nass, R., and Rao, R. (1998). Novel localization of a Na+/H+ exchanger in a late endosomal compartment of yeast. Implications for vacuole biogenesis. J. Biol. Chem. **273:** 21054–21060.

Nebenführ, A., Ritzenthaler, C., and Robinson, D.G. (2002). Brefeldin A: Deciphering an enigmatic inhibitor of secretion. Plant Physiol. **130:** 1102–1108.

Numata, M., and Orlowski, J. (2001). Molecular cloning and characterization of a novel (Na+,K+)/H+ exchanger localized to the trans-Golgi network. J. Biol. Chem. **276:** 17387–17394.

Ohgaki, R., Fukura, N., Matsushita, M., Mitsui, K., and Kanazawa, H. (2008). Cell surface levels of organellar Na+/H+ exchanger isoform 6 are regulated by interaction with RACK1. J. Biol. Chem. **283:** 4417–4429.

Orlando, D.A., Brady, S.M., Koch, J.D., Dinneny, J.R., and Benfey, P.N. (2009). Manipulating large-scale Arabidopsis microarray expression data: Identifying dominant expression patterns and biological process enrichment. In Methods in Molecular Biology, Methods and Protocols, Plant Systems Biology, D.A. Belostotsky, ed (New York: Humana Press), pp. 57–77.

Orlowski, J., and Grinstein, S. (2007). Emerging roles of alkali cation/proton exchangers in organellar homeostasis. Curr. Opin. Cell Biol. **19:** 483–492.

Pardo, J.M., Cubero, B., Leidi, E.O., and Quintero, F.J. (2006). Alkali cation exchangers: roles in cellular homeostasis and stress tolerance. J. Exp. Bot. **57:** 1181–1199.

Robert, S., Chary, S.N., Drakakaki, G., Li, S.D., Yang, Z.B., Raikhel, N.V., and Hicks, G.R. (2008). Endosidin1 defines a compartment involved in endocytosis of the brassinosteroid receptor BRI1 and the auxin transporters PIN2 and AUX1. Proc. Natl. Acad. Sci. USA **105:** 8464–8469.

Robinson, D.G., Jiang, L., and Schumacher, K. (2008). The endosomal system of plants: charting new and familiar territories. Plant Physiol. **147:** 1482–1492.

Rockwell, N.C., and Fuller, R.S. (2002). Specific modulation of Kex2/furin family proteases by potassium. J. Biol. Chem. **277:** 17531–17537.

Rodríguez-Rosales, M.P., Gálvez, F.J., Huertas, R., Aranda, M.N., Baghour, M., Cagnac, O., and Venema, K. (2009). Plant NHX cation/proton antiporters. Plant Signal. Behav. **4:** 265–276.

Rodriguez-Rosales, M.P., Jiang, X.Y., Gálvez, F.J., Aranda, M.N., Cubero, B., and Venema, K. (2008). Overexpression of the tomato K+/H+ antiporter LeNHX2 confers salt tolerance by improving potassium compartmentalization. New Phytol. **179:** 366–377.

Sade, N., Gebretsadik, M., Seligmann, R., Schwartz, A., Wallach, R., and Moshelion, M. (2010). The role of tobacco Aquaporin1 in improving water use efficiency, hydraulic conductivity, and yield production under salt stress. Plant Physiol. **152:** 245–254.

Samaj, J., Müller, J., Beck, M., Böhm, N., and Menzel, D. (2006). Vesicular trafficking, cytoskeleton and signalling in root hairs and pollen tubes. Trends Plant Sci. **11:** 594–600.

Samaj, J., Read, N.D., Volkmann, D., Menzel, D., and Baluska, F. (2005). The endocytic network in plants. Trends Cell Biol. **15:** 425–433.

Sanmartín, M., Ordóñez, A., Sohn, E.J., Robert, S., Sánchez-Serrano, J.J., Surpin, M.A., Raikhel, N.V., and Rojo, E. (2007). Divergent functions of VTI12 and VTI11 in trafficking to storage and lytic vacuoles in Arabidopsis. Proc. Natl. Acad. Sci. USA **104:** 3645–3650.

Shi, H., Ishitani, M., Kim, C., and Zhu, J.-K. (2000). The *Arabidopsis thaliana* salt tolerance gene SOS1 encodes a putative Na+/H+ antiporter. Proc. Natl. Acad. Sci. USA **97:** 6896–6901.

Shi, H., Quintero, F.J., Pardo, J.M., and Zhu, J.-K. (2002). The putative plasma membrane Na(+)/H(+) antiporter SOS1 controls long-distance Na(+) transport in plants. Plant Cell **14:** 465–477.

Shipman, R.L., and Inoue, K. (2009). Suborganellar localization of plastidic type I signal peptidase 1 depends on chloroplast development. FEBS Lett. **583:** 938–942.

Sohn, E.J., Kim, E.S., Zhao, M., Kim, S.J., Kim, H., Kim, Y.W., Lee, Y.J., Hillmer, S., Sohn, U., Jiang, L.W., and Hwang, I.W. (2003). Rha1, an Arabidopsis Rab5 homolog, plays a critical role in the vacuolar trafficking of soluble cargo proteins. Plant Cell **15:** 1057–1070.

Sottosanto, J.B., Gelli, A., and Blumwald, E. (2004). DNA array analyses of *Arabidopsis thaliana* lacking a vacuolar Na+/H+ antiporter: impact of AtNHX1 on gene expression. Plant J. **40:** 752–771.

Spalding, E.P., Hirsch, R.E., Lewis, D.R., Qi, Z., Sussman, M.R., and Lewis, B.D. (1999). Potassium uptake supporting plant growth in the absence of AKT1 channel activity: Inhibition by ammonium and stimulation by sodium. J. Gen. Physiol. **113:** 909–918.

Venema, K., Belver, A., Marin-Manzano, M.C., Rodríguez-Rosales, M.P., and Donaire, J.P. (2003). A novel intracellular K+/H+ antiporter related to Na+/H+ antiporters is important for K+ ion homeostasis in plants. J. Biol. Chem. **278:** 22453–22459.

Viotti, C., et al. (2010). Endocytic and secretory traffic in *Arabidopsis*

merge in the trans-Golgi network/early endosome, an independent and highly dynamic organelle. Plant Cell **22:** 1344–1357.

Xu, J., and Scheres, B. (2005). Dissection of Arabidopsis ADP-RIBOSYLATION FACTOR 1 function in epidermal cell polarity. Plant Cell **17:** 525–536.

Yamaguchi, T., Apse, M.P., Shi, H.Z., and Blumwald, E. (2003). Topological analysis of a plant vacuolar Na+/H+ antiporter reveals a luminal C terminus that regulates antiporter cation selectivity. Proc. Natl. Acad. Sci. USA **100:** 12510–12515.

Yamaguchi, T., Fukada-Tanaka, S., Inagaki, Y., Saito, N., Yonekura-Sakakibara, K., Tanaka, Y., Kusumi, T., and Iida, S. (2001). Genes encoding the vacuolar Na+/H+ exchanger and flower coloration. Plant Cell Physiol. **42:** 451–461.

Yamazaki, M., Shimada, T., Takahashi, H., Tamura, K., Kondo, M., Nishimura, M., and Hara-Nishimura, I. (2008). Arabidopsis VPS35, a retromer component, is required for vacuolar protein sorting and involved in plant growth and leaf senescence. Plant Cell Physiol. **49:** 142–156.

Yeung, E.C. (1999). The use of histology in the study of plant tissue culture systems - Some practical comments. In Vitro Cell. Dev. Biol. Plant **35:** 137–143.

Yokoi, S., Quintero, F.J., Cubero, B., Ruiz, M.T., Bressan, R.A., Hasegawa, P.M., and Pardo, J.M. (2002). Differential expression and function of *Arabidopsis thaliana* NHX Na+/H+ antiporters in the salt stress response. Plant J. **30:** 529–539.

Zouhar, J., Rojo, E., and Bassham, D.C. (2009). AtVPS45 is a positive regulator of the SYP41/SYP61/VTI12 SNARE complex involved in trafficking of vacuolar cargo. Plant Physiol. **149:** 1668–1678.